Immobilization of Enzymes by Electrochemical and Chemical Oxidative Polymerization of L-DOPA to Fabricate Amperometric Biosensors and Biofuel Cells

Mengzhen Dai, Lingen Sun, Long Chao, Yueming Tan, Yingchun Fu, Chao Chen, and Qingji Xie*

Key Laboratory of Chemical Biology and Traditional Chinese Medicine Research (Ministry of Education), National & Local Joint Engineering Laboratory for New Petrochemical Materials and Fine Utilization of Resources, College of Chemistry and Chemical Engineering, Hunan Normal University, Changsha 410081, China

S *Supporting Information*

ABSTRACT: Electrochemical/chemical oxidative synthesis and biosensing/biofuel cell applications of poly(L-DOPA) (PD) are studied versus polydopamine (PDA) as a recent hotspot biomaterial. The enzyme electrode developed by coelectrodeposition of PD and glucose oxidase (GOx), uricase, or tyrosinase shows biosensing performance superior to that of the corresponding PDA-based enzyme electrode. The chemical oxidative polymerization of L-DOPA (PD_C) by $NaAuCl_4$ in GOx-containing neutral aqueous solution is used to immobilize GOx and gold nanoparticles (AuNPs). The thus-prepared chitosan (CS)/GOx-PD_C-AuNPs/Au_{plate}/Au electrode working in the first-generation biosensing mode responds linearly to glucose concentration with a sensitivity of 152 μA mM^{-1} cm^{-2}, which is larger than those of the CS/GOx-PDA_C-AuNPs/Au_{plate}/Au electrode, the CS/GOx-poly(3-anilineboronic acid) (PABA)-AuNPs/Au_{plate}/Au electrode, and the most reported GOx-based enzyme electrodes. This PD_C-based enzyme electrode also works well in the second-generation biosensing mode and as an excellent bioanode in biofuel cell construction, probably because PD as an amino acid polymer has the higher biocompatibility and the more favorable affinity to the enzyme than PDA. The PD material of great convenience in synthesis, outstanding biocompatibility for preparing high-performance bionanocomposites, and strong capability of multifunctional coatings on many surfaces may find wide applications in diversified fields including biotechnology and surface-coating.

KEYWORDS: *electrochemical/chemical oxidative polymerization of L-DOPA, polymeric bionanocomposite, enzyme electrode, glucose biosensing, biofuel cell*
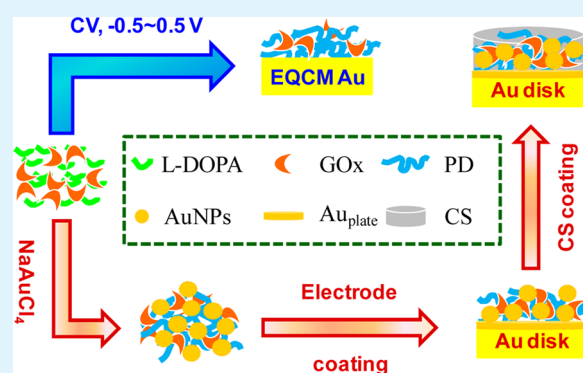
1. INTRODUCTION

Melanin is a biological pigment of high biomedical significance. It is one of the key factors of human skin color[1] and is also the molecular basis of diseases such as vitiligo, freckles, and melanoma.[2,3] There have been several comprehensive reviews on the behaviors and formation mechanisms of melanin in plants, insects, and marine animals.[4−8] It has been commonly accepted that tyrosinase catalyzes the oxidation of L-tyrosine to form 3-(3,4-dihydroxyphenyl)-L-alanine (L-DOPA, a rare amino acid), and melanin is finally formed.[7] Accordingly, melanin is actually poly(L-DOPA) (PD) as an amino acid polymer, which may be regarded as a special artificial "protein", though the chemical bonding for L-DOPA polymerization is not based on the peptide bond. In addition, L-DOPA is the gold standard in the therapy of Parkinson's disease.[9−11] Scientists have also studied the surface-adhesive characteristic of L-DOPA for versatile applications because the so-called mussel adhesive proteins contain L-DOPA at high concentrations, and thus, their adhesive functions are highly relevant to

L-DOPA.[12,13] Furthermore, L-DOPA has been used as a reducing agent and stabilizer for mediating the growth of Au nanoparticles (AuNPs) for analytical chemistry applications.[14,15] However, the electrochemical/chemical polymerization of L-DOPA for in situ immobilization of biomacromolecules to develop polymeric bionanocomposites (PBNCs) has not been addressed to date.

In contrast, since the inception of the polymer material of dopamine (DA, a structurally similar compound of L-DOPA) about 10 years ago,[16,17] polydopamine (PDA) and its PBNCs have been widely studied in diverse fields,[16−25] and up to date over 700 records can be found by a subject search on Web of Science (Thomson Reuters). PDA can be easily synthesized in solutions or on various types of inorganic and organic substrates. Typical PDA-synthesis methods include electro-

chemical oxidation,[16] chemical oxidation,[17,18] and enzymatic oxidation.[19] In view of the attractive features of facile synthesis, high biocompatibility, convenient chemical modification, good capability of surface-adhesion, etc., PDA and its PBNCs have been widely used in diverse areas including modification of surfaces,[20] immobilization of biomacromolecules,[18,21–23] biotechnology,[24] and environment analysis.[25] In addition, the uses of boronic-acid-group-bearing molecules or polymers to covalently immobilize glycoproteins are recently favored, which should less affect the protein bioactivity due to the covalent linking of boronic acid groups only at the glycosyl sites (reactions of boronic acid groups with 1,2- or 1,3-diols of glycoproteins to generate five or six-membered cyclic complexes),[26–28] as compared with immobilization of functional proteins by chemical bonding at the peptide chains.

Glucose is one of the most common analytes because millions of diabetics check their blood glucose levels daily. The electroanalytical methods can be used to quickly and sensitively analyze glucose. In general, the electroanalytical methods for monitoring glucose can be classified as nonenzymatic and enzymatic methods. The selectivity of nonenzymatic glucose sensors is relatively poor since some other sugars and endogenous interfering species can be oxidized near the potential for glucose oxidation, and the electrode activity can also be somewhat decreased by the adsorption of some relatively strong adsorbates like Cl^- anions and nonspecific proteins. In contrast, the enzymatic method can exhibit excellent selectivity, and glucose oxidase (GOx) is often used for amperometric sensing of glucose.[18,29,30] The immobilization of biomacromolecules with high load, high specific bioactivity, and high mass-transfer efficiency plays a key role in bioscience and biotechnology including biosensing and biofuel cell.[31–33] Immobilization of biomacromolecules at electrodes is the crucial step to construct various electrochemical biodevices, and the electrode is also the important experimental platform to study the redox activity of biomacromolecules. Generally, an organic polymer, even a typical conducting polymer like polyaniline,[34] shows only limited electron-conductivity versus excellent electron-conductors such as gold and graphite. Therefore, we often design PBNCs for various bioelectrochemical applications, which consist of a polymer, electron-conducting nanomaterials, and biomacromolecules and possess integrated properties and synergetic effects of the individuals.[28,35] The incorporation of electron-conducting nanoparticles can endow the nanocomposites with diverse functions, such as catalysis and electronics.[36] The PBNCs have been widely used to fabricate amperometric biosensors and other bioelectrochemical devices with improved performance.[37,38]

Herein, PD is chemically and electrochemically synthesized and used as an in situ enzyme-immobilization matrix for amperometric biosensor and biofuel cell applications. The polymerization of L-DOPA is studied in detail by in situ electrochemical quartz crystal microbalance (EQCM) and some other ex situ techniques. The involved enzymes include glucose oxidase (GOx), uricase (urate oxidase, UOx), and tyrosinase, and the enzyme electrode prepared by coelectrodeposition of PD and each of the three enzymes performs better than those by similar coelectrodeposition of PDA. A GOx-PD$_C$-AuNPs PBNC is also prepared through chemical oxidative polymerization of L-DOPA by NaAuCl$_4$ in the presence of GOx, and the enzyme electrode based on this PBNC possesses biosensing performance better than those based on similar PBNCs of PDA and poly(3-anilineboronic acid) (PABA) in the

first- and second-generation biosensing modes, which is also demonstrated as an excellent bioanode in biofuel cell construction.

2. EXPERIMENTAL SECTION

2.1. Instrumentation and Chemicals. Electrochemical experiments were conducted on a CHI660A electrochemical workstation (CH Instruments Co.) with a conventional three-electrode system. The Au disk electrode with 2.0 mm diameter (area = 0.031 cm^2) served as the working electrode (WE), a KCl-saturated calomel electrode (SCE) as the reference electrode (RE), and a carbon rod as the counter electrode (CE). All potentials reported here are cited versus SCE. However, the biofuel cell experiments were conducted on an Autolab PGSTA 30 electrochemical workstation (Eco Chemie BV, The Netherlands) with the GPES 4.9 software.[22,39,40] A computer-interfaced HP 4395A impedance analyzer was employed in the EQCM experiments, and AT-cut 9 MHz gold-coated piezoelectric quartz crystals (PQCs, 6.0 mm diameter Au electrode, 12.5 mm diameter quartz wafer, keyhole configuration, Model JA5, Beijing Chenjing Electronics Co., Ltd., China) were used.[31] UV−vis absorption spectra were collected on a UV2450 UV−vis spectrophotometer (Shimadzu Co., Japan). Transmission electron microscopy (TEM) images were collected on a JEM-2100F transmission electron microscope (Japan). Scanning electron microscopy (SEM) studies were performed on a Hitachi S4800 scanning electron microscope with a field emission electron gun.

GOx (EC 1.1.3.4; type II from *Aspergillus niger*, activity ≈ 150 U mg^{-1}, M_W ≈ 154 kDa), UOx (EC 1.7.3.3; from *Candida* sp, activity ≈ 4.7 U mg^{-1}, M_W ≈ 34 kDa), and tyrosinase (EC 1.14.18.1; 2.87 kU mg^{-1}, from *mushroom*, M_W ≈ 75 kDa) were purchased from Sigma. L-DOPA and DA were purchased from Aladdin, and 3-amino-phenylboronic acid (ABA) monohydrate and epinephrine were purchased from Sigma. HAuCl$_4$ was purchased from Tianjin Chemical Reagents Station (Tianjin, China). CS, glucose, galactose, acetaminophen, ascorbic acid, and uric acid were purchased from Sinopharm Chemical Reagent Co., Ltd. (Shanghai, China). *p*-Benzoquinone (BQ) and ferrocene monocarboxylic acid (FcMA) were purchased from Suzhou Time-Chem Technologies Co., Ltd. (Suzhou, China). Phosphate buffer solution (PBS) consisting of 0.10 M KH$_2$PO$_4$− K$_2$HPO$_4$ + 0.1 M K$_2$SO$_4$ (pH 7.0) served as the supporting electrolyte. CS (0.20 wt %) solution was prepared in 0.10 M acetate buffer solution (pH 5.4). All other chemicals were of analytical grade or better quality and used as received. Milli-Q ultrapure water (Millipore, ≥18 MΩ cm) was used throughout. All experiments were performed at room temperature around 25 °C.

2.2. Procedures. With the model enzyme GOx as a typical example, the preparation of enzyme electrodes based on PD is described in Scheme 1. First, the bare Au disk electrode was cleaned thoroughly according to the reported protocol.[41,42] The EQCM Au

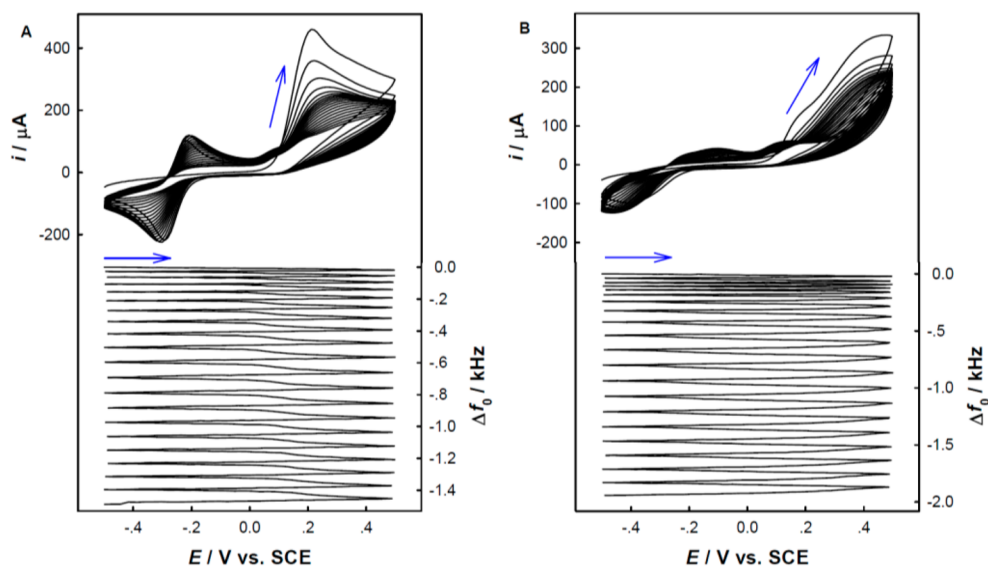**Scheme 1. Illustration of GOx Immobilization on the Electrode**
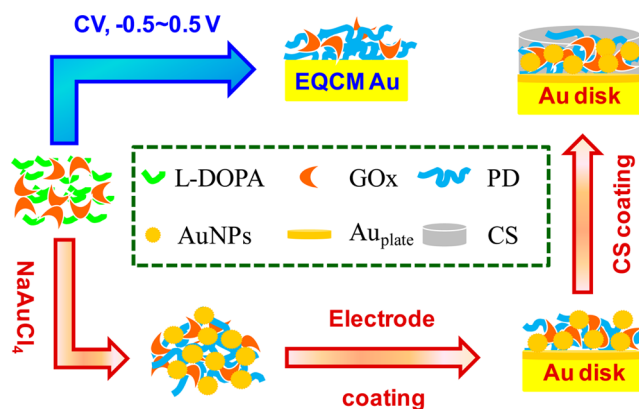
Figure 1. Simultaneous records of current (i) and Δf_0 during potential cycling of the EQCM Au electrode in 0.1 M PBS (pH 7.0) containing 10 mM L-DOPA (A) or 10 mM L-DOPA + 3.5 mg mL^{-1} GOx (B). Scan rate: 50 mV s^{-1}.

electrode was cleaned as reported before.[43] Afterward, the treated bare Au disk electrode was subjected to gold electroplating (Au$_{plate}$/Au) in 0.50 M aqueous H$_2$SO$_4$ containing 2.0 mM HAuCl$_4$ by multipotential-step electrolysis from 1.1 to 0 V vs SCE with a pulse width of 0.25 s, and the total time for the electrodeposition experiment was 225 s. The Au$_{plate}$/Au electrode has a larger real surface area and can show a better electrocatalytic performance toward electrooxidation of H$_2$O$_2$, as shown in Figure S1 (Supporting Information).

For the protocol of electrochemical oxidative polymerization of L-DOPA to form electrosynthesized PD (PD$_E$), cyclic voltammetry was conducted in a stirring PBS (pH 7.0) containing 10 mM L-DOPA monomer and 3.5 mg mL^{-1} GOx (optimized concentrations, vide infra) to form an enzyme film on an EQCM Au electrode (GOx-PD$_E$/EQCM Au). The GOx-PDA$_E$/EQCM Au electrode was prepared similarly to the GOx-PD$_E$/EQCM Au electrode, except that 10 mM DA was used instead. UOx-PD$_E$/EQCM Au electrode, UOx-PDA$_E$/EQCM Au electrode, tyrosinase-PD$_E$/EQCM Au electrode, and tyrosinase-PDA$_E$/EQCM Au electrode were prepared similarly to the GOx-PD$_E$/EQCM Au and GOx-PDA$_E$/EQCM Au cases, respectively, except that 0.77 mg mL^{-1} UOx or 1.7 mg mL^{-1} tyrosinase was used instead so that the molar concentration of UOx or tyrosinase is equal to that of GOx.

For the protocol of chemical oxidative polymerization of L-DOPA to form chemically synthesized PD (PD$_C$), 9.0 μL of 2.0 mM NaAuCl$_4$ was added into stirred 191 μL of PBS containing 10 mM L-DOPA and 2.5 mg mL^{-1} GOx. Precipitation of insoluble GOx-PD$_C$-AuNPs PBNC was visible at once. The reaction was allowed to occur for 5 h to maximize the precipitation, and the upper solution became rather clear. The GOx-PD$_C$-AuNPs precipitate was centrifuged and then redispersed in 100 μL of PBS, and 2.0 μL of the redispersed precipitate was cast-coated on the Au$_{plate}$/Au electrode. Then, 1.5 μL of 0.2 wt % CS solution was cast-coated to strengthen the enzyme film (CS/GOx-PD$_C$-AuNPs/Au$_{plate}$/Au). For comparison, 30 mM DA (optimized according to the biosensing sensitivity, as shown in Figure S2, Supporting Information) was used instead of 10 mM L-DOPA to go through the procedures similar to those described above, and the prepared electrode is denoted as CS/GOx-PDA$_C$-AuNPs/Au$_{plate}$/Au. It was observed that the rate of the redox reaction between DA and NaAuCl$_4$ is slower than that between L-DOPA and NaAuCl$_4$, as shown in Figure S3, Supporting Information. For comparison, a GOx-PD$_E$-AuNPs/Au$_{plate}$/Au electrode was also fabricated by cyclic voltammetry (−0.50−0.50 V vs SCE, 50 mV s^{-1}, 20 cycles) in an unstirred PBS solution containing 10 mM L-DOPA + 2.0 mM NaAuCl$_4$ + 3.5 mg mL^{-1} GOx. In addition, the CS/GOx-PABA-AuNPs/Au$_{plate}$/Au electrode was fabricated according to the reported

protocol.[28] The GOx-ABA composite was prepared by dissolving 10 mg of GOx and 5 mg of ABA in 1 mL of PBS and shaking the solution for 30 min to achieve reaction equilibrium. Then, 2.5 μL of GOx-ABA mixture and then 1.0 μL of 19.7 mM NaAuCl$_4$ were cast on the Au$_{plate}$/Au electrode for 40 min of reaction. Then, 1.5 μL of 0.2 wt % CS solution was cast-coated to strengthen the enzyme film and block the boronic sites in PABA (CS/GOx-PABA-AuNPs/Au$_{plate}$/Au). When not in use, the prepared enzyme electrodes were stored in a refrigerator at 4 °C as the dry state.

One unit of GOx activity (U) is defined as the production of 1 μmol H$_2$O$_2$ in 60 s under our experimental conditions, and the produced H$_2$O$_2$ is amperometrically detected. The enzymatic specific activity (ESA) can be written as ESA$_n$ = $n_{H_2O_2}$/m_{GOx},[31] where $n_{H_2O_2}$ in μmol is the molar quantity of H$_2$O$_2$ produced in the 60-s enzymatic reaction under our experimental conditions, and m_{GOx} in gram is the mass of GOx. The ESA of native solution-state GOx (ESA$_n$) and immobilized GOx (ESA$_i$) was evaluated by a well-established electrochemical method and EQCM method, respectively, and the enzymatic relative activity (ERA = ESA$_i$/ESA$_n$) for the immobilized enzyme can thus be worked out.[31,44] The operation details are given in Supporting Information, Figure S4.

In the first-generation biosensing mode, the fabricated enzyme electrodes were tested by potentiostating them at 0.70 V vs SCE in stirred PBS to detect the oxidation of enzymatically generated H$_2$O$_2$. The response current was marked with a change value between the steady-state current after substrate addition and the initial background current without substrate. Human serum samples used in this study were donated by Hunan Normal University Hospital. Prior to analysis, we diluted each of the serum samples by 10-fold using the supporting electrolyte (pH 7.0 PBS) without further pretreatments.[45,46] In the second-generation biosensing mode, cyclic voltammetry in quiescent solution was used for the mediator FcMA and chronoamperometry at 0.40 V vs SCE in stirred solution was used for the mediator BQ.

A monopolar glucose biofuel cell was constructed as an example to examine the energy-conversion performance of the enzymatic electrode, at which the CS/GOx-PD$_C$-AuNPs/Au$_{plate}$/Au electrode served as the bioanode in 20 mL of PBS containing 4.0 mM BQ and 60 mM glucose, and a Pt electrode served as the cathode in Nafion-membrane-isolated 0.40 M KMnO$_4$ + 0.60 M H$_2$SO$_4$ aqueous solution,[22] as shown in Scheme S1 (Supporting Information). The voltage (U_{cell}) and current density (j_{cell}) of the biofuel cell at varying external resistance loads (R_e) were dynamically monitored with the electrochemical noise module of the Autolab PGSTAT30 electro-chemical workstation (The Netherlands).[22,39,40]
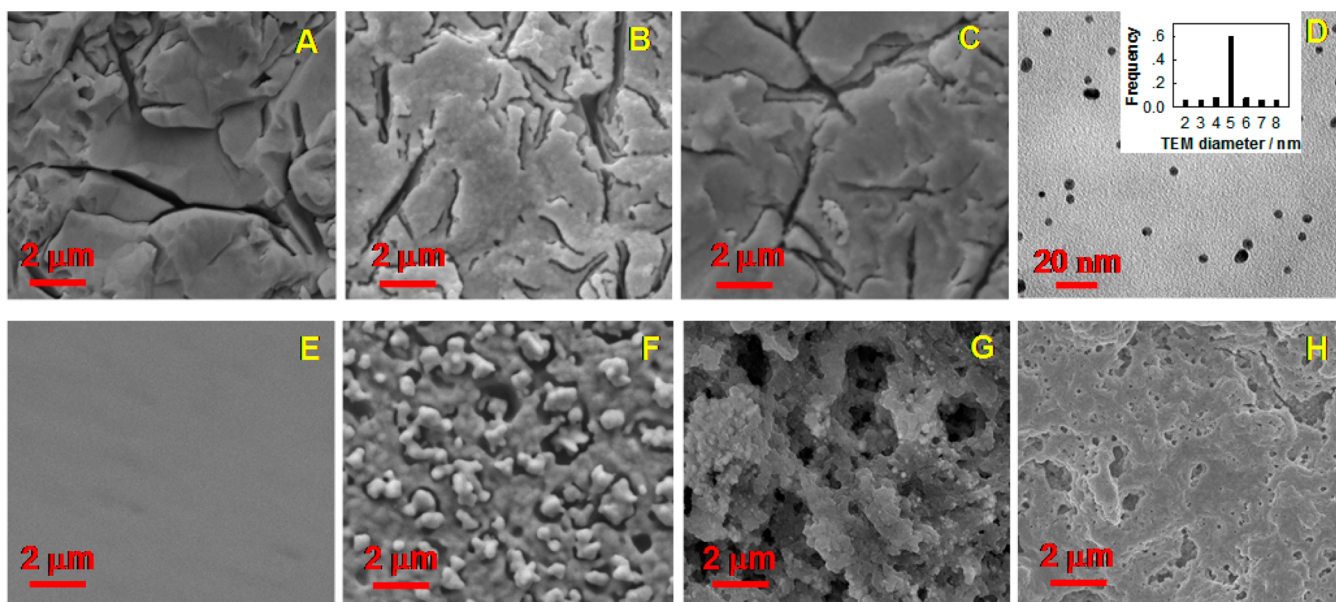
Figure 2. SEM pictures of bare EQCM Au (A), PD_E/EQCM Au (B), PD_E-GOx/EQCM Au (C), bare Au (E), Au_{plate}/Au (F), GOx-PD_C-AuNPs/Au_{plate}/Au (G), and CS/GOx-PD_C-AuNPs/Au_{plate}/Au (H) electrode surfaces. TEM image of the GOx-PD_C-AuNPs bionanocomposite (D).

3. RESULTS AND DISCUSSION

3.1. Electropolymerization of L-DOPA and Fabrication of the Enzyme Electrodes. Figure 1A shows the EQCM response to potential cycling on a bare EQCM Au electrode in neutral PBS (pH 7.0) containing 10 mM L-DOPA. An L-DOPA-oxidation current peak was observed at ca. 0.2 V vs SCE in the first positive scan, but the corresponding reduction current peak roughly at ca. 0.1 V vs SCE was negligibly small, probably because the oxidation product of L-DOPA was so easily transformed to its intramolecular cyclization product under our experimental conditions. Interestingly, a new pair of redox peaks roughly at −0.2/−0.3 V vs SCE appeared. All of the current peaks became lowered cycle by cycle, indicating a gradual decrease in the electrode activity due to the deposition of an insulating PD layer (PD_E). The frequency decreased cycle by cycle, indicating electropolymerization of L-DOPA and the polymer deposition on the electrode. The total net frequency decrease after 20 potential cycles was 1.49 kHz. The possible mechanism is given in Scheme S2 (Supporting Information), which is similar to the reported ECECEE mechanism for DA electrochemistry[16] and the reported biooxidation mechanism for L-DOPA. Briefly, L-DOPA is electrooxidized to L-dopaquinone (L-DOPAQ, $E_{pa} \approx 0.2$ V vs SCE), and the intramolecular cyclization reaction of L-DOPAQ via 1,4-Michael addition leads to the formation of the more readily oxidized L-dopachrome (L-DOPAC, $E_{pa} \approx -0.2$ V vs SCE). The L-DOPAC can further undergo indole-like polymerization on the electrode, yielding a deposited melanin polymer.[16,47] Figure 1B shows the EQCM response on a bare EQCM Au electrode during cyclic voltammetry in neutral PBS (pH 7.0) containing 10 mM L-DOPA and 3.5 mg mL^{-1} GOx. L-DOPA-oxidation current peaks were observed near ca. 0.2 and 0.4 V vs SCE in the first positive scan, a cathodic peak roughly at ca. −0.4 V vs SCE was recorded in the negative scan, and a new oxidation peak (ca. −0.2 V vs SCE) was obtained in the second positive scan. The current peaks were also lowered cycle by cycle due to the deposition of the insulating polymer composite layer. The frequency also decreased cycle by cycle, and the total

net frequency decrease after 20 potential cycles was 1.94 kHz. In comparison with the GOx-free case, a $-\Delta f_0$ response greater by 0.450 kHz was observed under comparable polymerization conditions, which should correspond to the GOx immobilized in the PD_E film. It is interesting that the cyclic voltammetry profile in the presence of GOx notably differed from that in the absence of GOx, namely, the redox peaks are much poorly shaped in the former case than in the latter case (even in the first potential cycle), which may imply the presence of some notable molecular interactions between L-DOPA (or its oxidation products) and GOx. We believe that such molecular interactions may result from the strong electrostatic interactions, hydrogen bonding, and/or nucleophilic reaction (i.e., amino groups of the protein nucleophilically attack the quinone products after L-DOPA oxidation) between L-DOPA (or its oxidation products) and GOx, as discussed later.

Figure S5A (Supporting Information) shows the EQCM response on a bare EQCM Au electrode during cyclic voltammetry in neutral PBS (pH 7.0) containing 10 mM DA. A DA-oxidation current peak was observed at ca. 0.3 V vs SCE in the first positive scan, and the corresponding reduction current peak roughly at 0.05 V vs SCE was much smaller but clearly visible, because the oxidation product of DA was mostly transformed to its intramolecular cyclization product under our experimental conditions. A cathodic peak roughly at ca. −0.35 V vs SCE was recorded in the negative scan, and a new oxidation peak (ca. −0.2 V vs SCE) was obtained in the second positive scan. The current peaks were lowered cycle by cycle also due to the deposition of an insulating polymer layer (PDA_E). The total net frequency decrease after 20 potential cycles was 612 Hz, which is notably smaller than that in the L-DOPA case (1.49 kHz, Figure 1A). This finding should indicate that the electropolymerization rate of DA is notably slower than that of L-DOPA, supporting the experimental finding given in Figure S3 (Supporting Information). The possible mechanism is shown in Scheme S2 (Supporting Information).[16] Figure S5B (Supporting Information) shows the EQCM response on a bare EQCM Au electrode during cyclic voltammetry in neutral PBS (pH 7.0) containing 10 mM DA and 3.5 mg mL^{-1} GOx.
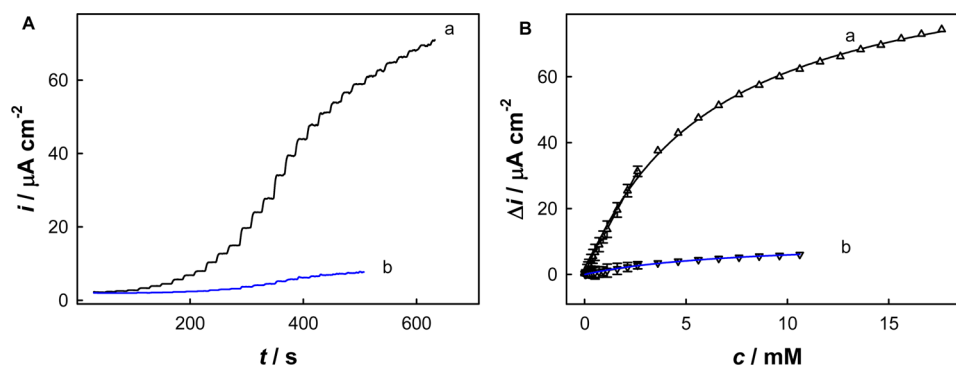
Figure 3. Chronoamperometric responses (A) to successive additions of glucose and the calibration curves (B) on GOx-PD$_E$/EQCM Au (a), and GOx-PDA$_E$/EQCM Au (b) electrodes at 0.7 V vs SCE in pH 7.0 PBS. The long solid curves in panel B show the nonlinear least-squares fitting of the experimental Δi vs c data to the Michaelis−Menten equation, which can yield the apparent Michaelis−Menten constants (K_m^{app}) listed in Table 1 (vide infra).

The cyclic voltammetry and frequency profiles are basically similar to those in the GOx-free case. The total net frequency decrease after 20 potential cycles was 651 Hz. In comparison with the GOx-free case, a greater $-\Delta f_0$ by 39 Hz was observed under comparable polymerization conditions, which should also correspond to the GOx immobilized in the PDA$_E$ film. In comparison with the PD$_E$ case, the PDA$_E$ case here gave a notably smaller difference of the cyclic voltammetry profiles in the presence and absence of GOx, which implies that the molecular interactions between L-DOPA (or its oxidation products) and GOx are notably stronger than those between DA (or its oxidation products) and GOx.

The SEM pictures for the EQCM Au electrodes are shown in Figure 2. The bare EQCM Au electrode (A) shows a relatively smooth surface with some cracks (unpolished quartz crystals employed here). After electrodeposition of PD$_E$ and GOx-PD$_E$ on the EQCM Au electrode (B and C), we can see very thin films on the electrode. Furthermore, cyclic voltammetry and electrochemical impedance spectroscopy were also used to characterize the modified EQCM Au electrodes in the presence of an electroactive Fe(CN)$_6^{3-/4-}$ redox probe, as shown in Figure S6 (Supporting Information). Both the electrochemical impedance spectroscopy and cyclic voltammetry results have indicated the successful chemical modifications on the EQCM Au electrode surface.

Figure 3 shows the amperometric responses and calibration curves of GOx-PD$_E$/EQCM Au and GOx-PDA$_E$/EQCM Au electrodes under optimized conditions in the first-generation biosensing mode. The response at the GOx-PD$_E$/EQCM Au electrode is linear with glucose concentration from 2.0 μM to 2.7 mM (R^2 = 0.998), with a sensitivity of 48.6 μA mM^{-1} cm^{-2} and a limit of detection (LOD, S/N = 3) of 0.8 μM. The response at the GOx-PDA$_E$/EQCM Au electrode is linear with glucose concentration from 50 μM to 2.6 mM (R^2 = 0.998), with a sensitivity of 10.4 μA mM^{-1} cm^{-2} and a LOD (S/N = 3) of 10 μM, as listed in Table 1. Obviously, the sensitivity of the GOx-PD$_E$/EQCM Au electrode is better than that of the GOx-PDA$_E$/EQCM Au electrode, suggesting that the use of PD material is a more promising solution for enzymatic trace analysis of some low-concentration analytes than the use of PDA material. In fact, the L-DOPA self-polymerization (virtually oxygen driven) can occur on organic (e.g., plastic), conducting inorganic (e.g., aluminum wire), and nonconducting inorganic (e.g., tagboard) materials, and the PD films can be robustly attached to the surfaces of plastic, aluminum wire, and

Table 1. Characteristics of GOx-PD$_E$/EQCM Au and GOx-PDA$_E$/EQCM Au Electrodes Prepared under Optimized Conditions

enzyme electrode	GOx-PD$_E$/EQCM Au	GOx-PDA$_E$/EQCM Au
LDR (mM)	0.002−2.7	0.05−2.6
sensitivity (μA mM^{-1} cm^{-2})	48.6	10.4
LOD (μM)	0.8	10
K_m^{app} (mM)	6.3	7.8
ESA$_i$ (kU g^{-1})	17	10
ERA (%)	43 ± 1	25 ± 1

tagboard (Figure S7, Supporting Information), implying that the L-DOPA polymerization, just like the PDA case,[17] is also favorable for convenient preparation of PD-based multifunctional coatings on various substrates. Hence, the polymer−substrate interactions may be equally good in the PD and PDA case, and the better biosensing performance in the PD case should result from the higher biocompatibility and favorable intermolecular interactions of the GOx and PD-system as mentioned above.

ESA values of the native and immobilized GOx were quantitatively estimated via electrochemical and EQCM methods, as discussed in the Supporting Information and summarized in Table 1. We obtain ESA$_i$ = 17 ± 1 kU g^{-1} for the immobilized GOx on GOx-PD$_E$/EQCM Au enzyme electrode and ESA$_i$ = 10 ± 1 kU g^{-1} for the immobilized GOx on GOx-PDA$_E$/EQCM Au enzyme electrode. The later ESA$_i$ result for the GOx-PDA$_E$/EQCM Au electrode agrees well with that in our previous report.[21] The greater ESA$_i$ in the PD case should confirm the higher biocompatibility of PD than PDA, perhaps because PD is an amino acid polymer like artificial "protein" and thus intrinsically possesses a higher biocompatibility and/or some stronger and but favorable molecular interactions between L-DOPA and GOx.

The electrosynthesized PD material also can immobilize other enzymes to prepare enzyme electrodes of biosensing performance superior to the electrosynthesized PDA material. The immobilization of UOx and tyrosinase was examined here as an example. Figure S8 (Supporting Information) shows the EQCM response on bare EQCM Au electrode during cyclic voltammetry in neutral PBS (pH 7.0) containing 10 mM L-DOPA (A), 10 mM L-DOPA + 0.77 mg mL^{-1} UOx (B), 10 mM L-DOPA + 1.7 mg mL^{-1} tyrosinase (C), 10 mM DA (D), 10 mM DA + 0.77 mg mL^{-1} UOx (E), or 10 mM DA + 1.7 mg

mL^{-1} tyrosinase (F). In comparison with the PD$_E$ case, the difference of the cyclic voltammetry profiles in the presence and absence of UOx (or tyrosinase) was somewhat smaller in the PDA$_E$ case, also implying that molecular interactions between L-DOPA (or its oxidation product) and UOx (or tyrosinase) are stronger than those between DA (or its oxidation product) and UOx. tyrosinase can catalyze the polymerization of both L-DOPA and DA; thus, their cyclic voltammetry profiles in the absence of tyrosinase are notably different from those in the presence of tyrosinase. It should be noted that the cyclic voltammetry profiles of L-DOPA are notably different in the presence of GOx or UOx, probably indicating some unique molecular interaction between L-DOPA and GOx or UOx, though such interactions are not well understood at present and require detailed studies in the future. As shown in Figure S9 and Table S1 (Supporting Information), the amperometric response at the UOx-PD$_E$/EQCM Au electrode is linear with UA concentration from 0.1 μM to 2.5 mM (R^2 = 0.998), with a sensitivity of 164 μA mM^{-1} cm^{-2} and a LOD (S/N = 3) of 0.08 μM. The response at the UOx-PDA$_E$/EQCM Au electrode is linear with UA concentration from 2.0 μM to 2.5 mM (R^2 = 0.998), with a sensitivity of 42.8 μA mM^{-1} cm^{-2}, and a LOD (S/N = 3) of 1 μM. The response at the tyrosinase-PD$_E$/EQCM Au electrode is linear with catechol concentration from 0.4 μM to 2.1 mM (R^2 = 0.998), with a sensitivity of 107 μA mM^{-1} cm^{-2} and a LOD (S/N = 3) of 0.03 μM. The response at the tyrosinase-PDA$_E$/EQCM Au electrode is linear with catechol concentration from 1.0 μM to 1.6 mM ((R^2 = 0.998), with a sensitivity of 54.3 μA mM^{-1} cm^{-2} and a LOD (S/N = 3) of 0.4 μM. The biosensing performance at the UOx-PD$_E$/EQCM Au electrode and the tyrosinase-PD$_E$/EQCM Au electrode is much better than that at the UOx-PDA$_E$/EQCM Au electrode and the tyrosinase-PDA$_E$/EQCM Au electrode, respectively, highlighting that L-DOPA is an excellent "monomer" for the preparation of polymeric enzyme films for biosensing applications.

3.2. Chemical Oxidative Polymerization of L-DOPA and Fabrication of the Enzyme Electrodes.

NaAuCl$_4$ was used here as a chemical oxidant to polymerize L-DOPA (PD$_C$) in aqueous solution in the presence of GOx, and many conducting AuNPs could be produced simultaneously. UV–vis spectrophotometry was used to monitor the formation of the PBNCs. As shown in Figure 4, L-DOPA and GOx gave an absorption peak at 280 nm, and one new absorption band
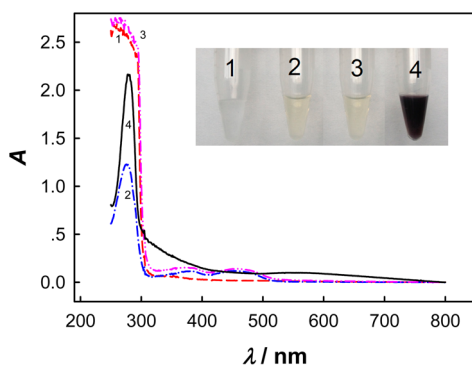
Figure 4. UV–vis absorption spectra and a digital picture of 10 mM L-DOPA (red curve, 1), 2.5 mg mL^{-1} GOx (blue curve, 2), 2.5 mg mL^{-1} GOx + 10 mM L-DOPA (pink curve, 3), and 2.5 mg mL^{-1} GOx + 10 mM L-DOPA + 2 mM NaAuCl$_4$ (black curve, 4) in 0.1 M PBS (pH 7.0).

peaking at about 530 nm could be observed after NaAuCl$_4$ addition. The inset of Figure 4 shows the visual inspection results. As soon as NaAuCl$_4$ was added into the transparent and colorless GOx + L-DOPA aqueous solution, the solution turned turbid and red brown in color, indicating the immediate onset of L-DOPA oxidation/polymerization and AuNPs formation, but more precipitates were formed after 5 h in the presence of GOx, implying the formation of three-component GOx-PD$_C$-AuNP bionanocomposite. The TEM image of the GOx-PD$_C$-AuNP bionanocomposite is shown in Figure 2D, which shows that the bionanocomposite contains many Au nanoparticles of a statistically dominant size of 5 nm.

SEM pictures have given the visual results and evidence for successful electrode modification, as shown in Figure 2. The bare Au disk electrode shows a rather smooth surface (E). After electrodeposition of Au on the Au disk electrode (F), many small-sized Au particles (ca. 500 nm) are clearly seen. After cast-coating the GOx-PD$_C$-AuNPs bionanocomposite on the Au$_{plate}$/Au disk electrode (G), we can clearly observe a blanket of many surface nanoparticles. After cast-coating the CS film on the GOx-PD$_C$-AuNPs/Au$_{plate}$/Au disk electrode (H), the outer surface was newly covered with a glue-like film. Furthermore, cyclic voltammetry and electrochemical impedance spectroscopy were also used to characterize the modified Au disk electrodes in the presence of electroactive Fe(CN)$_6^{3-/4-}$ redox probe, as shown in Figure S10 (Supporting Information). The electrochemical impedance spectroscopy and cyclic voltammetry results here both confirm various successful surface modifications for preparing the enzyme electrode.

To obtain the best sensitivity for the glucose assay, various conditions for enzyme electrode fabrication and biosensing experiments have been optimized according to the biosensing signal output through variation of the examined one while fixing the others, as shown in Figure S11 (Supporting Information). We finally obtained optimized conditions for enzyme electrode fabrication as follows: 2.5 mg mL^{-1} GOx, 10 mM L-DOPA, 2 mM NaAuCl$_4$, and 1.5 μL 0.20 wt % CS. The optimized parameters for biosensing experiments are pH 7.0 PBS test solution and sensing potential at 0.7 V vs SCE (H$_2$O$_2$-oxidation mode).

To test the performance of the biosensors, the steady-state currents for several enzyme electrodes under optimized conditions were examined in stirred PBS in the first-generation biosensing mode. Figure 5 shows the amperometric glucose-biosensing responses (A) and the calibration curves (B) of several enzyme electrodes. The response at the CS/GOx-PD$_C$-AuNPs/Au$_{plate}$/Au electrode is linear with glucose concentration from 2.0 μM to 3.4 mM (R^2 = 0.998), with a sensitivity of 152 μA mM^{-1} cm^{-2} and a LOD (S/N = 3) of 0.1 μM. Fast and sensitive response toward glucose reaches steady-state within 5 s. Our CS/GOx-PD$_C$-AuNPs/Au$_{plate}$/Au electrode (152 μA mM^{-1} cm^{-2}) shows the highest sensitivity as compared with CS/GOx-PDA$_C$-AuNPs/Au$_{plate}$/Au (95.5 μA mM^{-1} cm^{-2}), CS/GOx-PABA-AuNPs/Au$_{plate}$/Au (116 μA mM^{-1} cm^{-2}), and GOx-PD$_E$-AuNPs/Au$_{plate}$/Au (41.7 μA mM^{-1} cm^{-2}) electrodes as well as many reported results (Table 2). Since PD is an amino acid polymer like an artificial "protein" and thus exhibits very high biocompatibility to more effectively entrap highly bioactive GOx, and AuNPs can be produced near/on the enzyme molecule after NaAuCl$_4$ addition, the electron transfer of the enzymatic reaction and the amperometric sensitivity can be greatly promoted here.
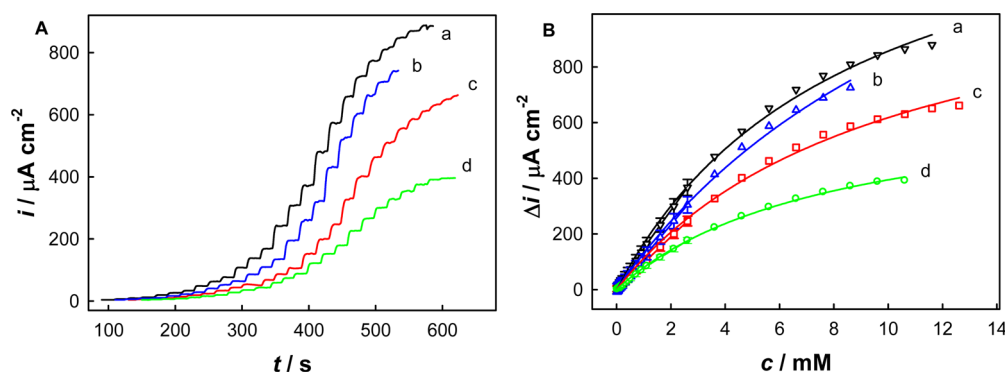
Figure 5. Chronoamperometric responses (A) to successive additions of glucose and the calibration curves (B) on CS/GOx-PD$_C$-AuNPs/Au$_{plate}$/Au (a), CS/GOx-PABA-AuNPs/Au$_{plate}$/Au (b), CS/GOx-PDA$_C$-AuNPs/Au$_{plate}$/Au (c), and GOx-PD$_E$-AuNPs/Au$_{plate}$/Au (d) electrodes at 0.7 V vs SCE in pH 7.0 PBS.

Table 2. Construction and Performance of Some Typical GOx-Based Glucose Biosensors Using AuNPs[a]

fabrication	sensitivity (μA mM^{-1} cm^{-2})	LOD (μM)	LDR (mM)	ref
AuNPs-GOx-Nafion/GCE	0.4	370	1−20	48
CS/GOx-PABA-Au$_{nano}$/Au$_{plate}$/Au	97.7	0.1	0.002−3.7	28
GOx/cystamine/Au/dithiol/Au	8.8	8.2	0.02−5.7	49
CS-GOx-AuNP/Au		2.7	0.005−2.4	50
GOx-graphene/PANI/AuNP/GCE		0.6	0.004−1.1	51
GOx/AuNPs/graphene/CNTs/GCE	29.7	4.8	0.005−0.2	52
Nafion/GOx/Au-MWNT/GCE	5.7	20	0.05−22	53
GOx-PD$_E$-AuNPs/Au$_{plate}$/Au	41.7	1.0	0.005−2.8	this work
CS/GOx-PABA-AuNPs/Au$_{plate}$/Au	116	0.2	0.002−3.4	this work
CS/GOx-PDA$_C$-AuNPs/Au$_{plate}$/Au	95.5	0.2	0.005−2.5	this work
CS/GOx-PD$_C$-AuNPs/Au$_{plate}$/Au	152	0.1	0.002−3.4	this work

[a]GCE, glassy carbon electrode; PB, Prussian blue; MWNT, multiwalled carbon nanotube; CNTs, carbon nanotubes; PANI, poly(aniline).
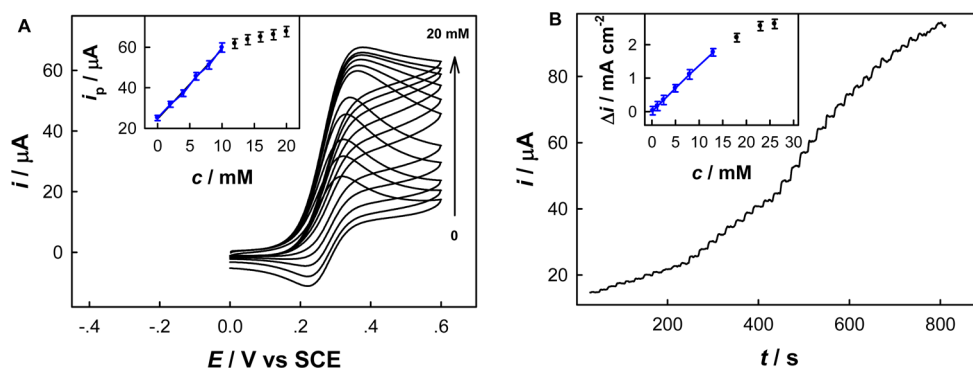

Figure 6. (A) Cyclic voltammogram and the calibration curve of the anodic peak current (insert) of a CS/GOx-PD$_C$-AuNPs/Au$_{plate}$/Au electrode in PBS containing 4 mM FcMA and 0, 2, 4, 6, 8, 10, 12, 14, 16, 18, or 20 mM glucose. Scan rate: 50 mV s^{-1}. (B) Chronoamperometric responses to successive additions of glucose and the calibration curve (insert) of a CS/GOx-PD$_C$-AuNPs/Au$_{plate}$/Au electrode at 0.4 V vs SCE in degassed PBS containing 4 mM BQ.

The apparent Michaelis−Menten constant (K_m^{app}) is an indicator of the enzyme−substrate kinetics, which can be calculated from the Michaelis−Menten equation, $\Delta i = \Delta i_{max} c / (K_m^{app} + c)$ (here Δi is the steady-state current response after the addition of substrate, Δi_{max} is the maximum current response under saturated substrate conditions, and c in mM is the concentration of substrate). As shown in Figure 5, we fit the experimental Δi vs c data to the Michaelis−Menten equation according to the nonlinear least-squares fitting algorithm embedded in SigmaPlot Scientific Graphing Software, version 10.0, and obtain the value of K_m^{app} for the CS/GOx-PD$_C$-AuNPs/Au$_{plate}$/Au electrode as 4.5 mM, which is lower than the

reported values of 7.2 mM for the GOx immobilized at an AuNPs modified TiO$_2$ nanotube array electrode, implying that the immobilized GOx here possesses high enzymatic activity and affinity to glucose.[54]

The anti-interference ability of the CS/GOx-PD$_C$-AuNPs/Au$_{plate}$/Au electrode was also examined. As shown in Figure S12A (Supporting Information), the additions of 1.0 mM galactose, 0.1 mM uric acid, and 0.1 mM acetaminophen caused very small interferences to the detection of 1.0 mM glucose, and the additions of 0.1 M NaCl, 0.1 mM ascorbic acid (AA), 0.1 mM epinephrine, 0.1 M KCl, and 1.0 mM acetate caused no interferences. The reproducibility and storage stability of the
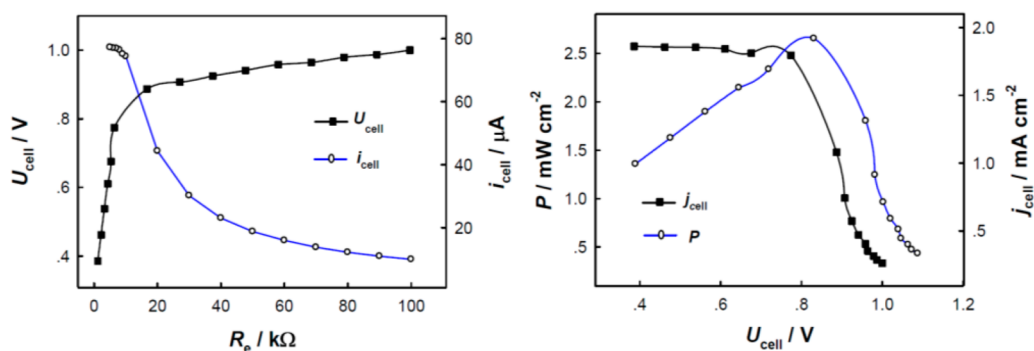
Figure 7. i_{cell} and U_{cell} as functions of R_e as well as j_{cell} and P as functions of U_{cell} for the monopolar biofuel cell fabricated as detailed in the text.

biosensor were investigated by amperometric measurements. The reproducibility of this biosensor was evaluated with a relative standard deviation of 4.5% ($n = 5$) for 1 mM glucose. Our electrode maintained 85% of its initial current response after 15 days (Figure S12B, Supporting Information). The potential of practical usage of the biosensor was validated with several human serum samples, and the values measured at the CS/GOx-PD$_C$-AuNPs/Au$_{plate}$/Au electrode agreed well with the hospital results (Table S2, Supporting Information).

3.3. Biosensing Performance in the Second-Generation Biosensing Mode and Biofuel Cell Fabrication. It is well known that the concentration of dissolved O_2 in aqueous solutions is rather small ($\sim$1 mM); thus, the linear detection range (LDR) of the first generation amperometric electrode is limited for high-concentration glucose, which may restrict the convenient use for the direct assay of blood glucose at the micromolar level.[30] Hence, the biosensor was also used to determine glucose in the second-generation biosensing mode with the solution-state redox mediator of BQ or FcMA at relatively high concentration. As shown in Figure 6A, 4 mM FcMA exhibited well-defined redox peaks centering at ca. 0.3 V vs SCE on the CS/GOx-PD$_C$-AuNPs/Au$_{plate}$/Au electrode, and successive additions of glucose increased the anodic currents and decreased the cathodic currents near the redox peaks, and the anodic peak current is linear with the glucose concentration (insert), highlighting the mediator effect of FcMA on GOx. Here, in the presence of 4 mM FcMA, the LDR was favorably extended to 12 mM with a slope of 11.3 μA mM^{-1} cm^{-2}, as compared with the first-generation biosensing mode. The current responses and the calibration curves of the CS/GOx-PD$_C$-AuNPs/Au$_{plate}$/Au electrode to glucose in the presence of 4 mM BQ at a detection potential of 0.4 V are shown in Figure 6B. The LDR was favorably extended to 15 mM with a sensitivity as high as 140 μA mM^{-1} cm^{-2}. The above results demonstrate that this biosensor can evolve into second-generation biosensors with a wider LDR by simple addition of a redox mediator in the detection solution.

Since the CS/GOx-PD$_C$-AuNPs/Au$_{plate}$/Au electrode worked well in the presence of 4 mM BQ, the biofuel cell application potential of this enzyme electrode was examined. The constructed monopolar biofuel cell is schematically shown in Scheme S1 (Supporting Information). As shown in Figure 7, the biofuel cell exhibited an open-circuit potential of ca. 1.0 V, a short-circuit current of 2.58 mA cm^{-2}, and a maximum power density (P_{max}) of 2.62 mW cm^{-2}. This P_{max} is much larger than most reported values,[39,45,55−58] indicating that the enzyme film here is an excellent anodic material for biofuel cell development.

4. CONCLUSIONS

In summary, we have described that the enzyme electrode developed by coelectrodeposition of PD and GOx, UOx, or tyrosinase shows biosensing performance superior to that of the corresponding enzyme electrode using the electrosynthesized PDA material. The chemical oxidative polymerization of L-DOPA by NaAuCl$_4$ in GOx-containing neutral aqueous solution was also used to immobilize GOx and AuNPs. The thus-prepared enzyme electrode gave a glucose assay sensitivity higher than that in the cases using chemically synthesized PDA and PABA materials and also worked well for biofuel cell construction. Considering the fact that L-DOPA has an additional −COOH group versus DA and that the polymerization rate of L-DOPA is faster than that of DA, the multifunctional coatings based on PD should be superior to those based on DA at least in two aspects, i.e., additional capability of −COOH-based chemical modification and better time-effectiveness in operation. Therefore, artificial synthesis of the biopolymer and its bionanocomposites based on L-DOPA should be promising for many other applications in diverse fields including biotechnology and surface-coating.

■ ASSOCIATED CONTENT

ⓈSupporting Information

Preparation and performance of the enzyme electrodes; polymerization mechanism; operation details for the measurement of enzymatic specific activity; and schematic diagram of the glucose biofuel cell. The Supporting Information is available free of charge on the ACS Publications website at DOI: 10.1021/acsami.5b01865.

■ AUTHOR INFORMATION

Corresponding Author

*E-mail: xieqj@hunnu.edu.cn.

Notes

■ ACKNOWLEDGMENTS

■ REFERENCES

(1) Smith, K.; Blois, M. The Melanins: Their Synthesis and Structure. In *Photochemical and Photobiological Reviews*; Springer: New York, 1978; pp 115−134.

(2) Herz, W.; Falk, H.; Kirby, G. W.; Roy, S. Melanin, Melanogenesis, and Vitiligo. In *Progress in the Chemistry of Organic Natural Products*; Springer: Vienna, Austria, 2007; pp 131−185.

(3) Porta, G. D.; Muhlbock, O.; Robson, N. C.; Swan, G. A. Studies on the Structure of Some Synthetic Melanins. In *Structure and Control of the Melanocyte*; Springer: Berlin, Germany, 1966; pp 155−162.

(4) Raper, H. S. The Aerobic Oxidases. *Phys. Rev.* **1928**, 8, 245−282.

(5) Jimbow, K.; Quevedo, W. C., Jr.; Fitzpatrick, T. B.; Szabo, G. Some Aspects of Melanin Biology: 1950−1975. *J. Invest. Dermatol.* **1976**, 67, 72−89.

(6) Fitzpatrick, T. B.; Becker, S. W.; Lerner, A. B.; Montgomery, H. Tyrosinase in Human Skin: Demonstration of Its Presence and of Its Role in Human Melanin Formation. *Science* **1950**, 112, 223−225.

(7) Mason, H. S. The Chemistry of Melanin: III. Mechanism of the Oxidation of Dihydroxyphenylalanine by Tyrosinase. *J. Biol. Chem.* **1948**, 172, 83−99.

(8) Arnow, L. E. Colorimetric Determination of the Components of 3,4-Dihydroxyphenylalaninetyrosine Mixtures. *J. Biol. Chem.* **1937**, 118, 531−537.

(9) Sotnikova, T. D.; Beaulieu, J.-M.; Barak, L. S.; Wetsel, W. C.; Caron, M. G.; Gainetdinov, R. R. Dopamine-Independent Locomotor Actions of Amphetamines in a Novel Acute Mouse Model of Parkinson Disease. *PLoS Biol.* **2005**, 3, 271.

(10) McDowell, F.; Lee, J. E.; Swift, T.; Sweet, R. D.; Ogsbury, J. S.; Kessler, J. T. Treatment of Parkinson's Syndrome with L Dihydroxyphenylalanine (Levodopa). *Ann. Int. Med.* **1970**, 72, 29−35.

(11) Mercuri, N. B.; Bernardi, G. The Lagical of L-dopa: Why is it the Gold Standard Parkinson's Disease Therapy? *Trends Pharmacol. Sci.* **2005**, 26, 341−344.

(12) Waite, J. H.; Tanzer, M. L. The Bioadhesive of Mytilus Byssus: A Protein Containing L-DOPA. *Biochem. Biophys. Res. Commun.* **1980**, 96, 1554−1561.

(13) Waite, J. H.; Tanzer, M. L. Polyphenolic Substance of *Mytilus edulis*: Novel Adhesive Containing L-Dopa and Hydroxyproline. *Science* **1981**, 212, 1038−1040.

(14) Lu, C.; Zhang, M.; Li, A.; He, X.; Yin, X. 3,4-Dihydroxy-L-Phenylalanine for Preparation of Gold Nanoparticles and as Electron Transfer Promoter in H_2O_2 Biosensor. *Electroanalysis* **2011**, 23, 2421−2428.

(15) Baron, R.; Zayats, M.; Willner, I. Dopamine-, L-DOPA-, Adrenaline-, and Noradrenaline-Induced Growth of Au Nano-particles:An Assays for the Detection of Neurotransmitters and of Tyrosinase Activity. *Anal. Chem.* **2005**, 77, 1566−1571.

(16) Li, Y.; Liu, M.; Xiang, C.; Xie, Q.; Yao, S. Electrochemical Quartz Crystal Microbalance Study on Growth and Property of the Polymer Deposit at Gold Electrodes during Oxidation of Dopamine in Aqueous Solutions. *Thin Solid Films* **2006**, 497, 270−278.

(17) Lee, H.; Dellatore, S. M.; Miller, W. M.; Messersmith, P. B. Mussel-Inspired Surface Chemistry for Multifunctional Coatings. *Science* **2007**, 318, 426−430.

(18) Fu, Y.; Li, P.; Xie, Q.; Xu, X.; Lei, L.; Chen, C.; Zou, C.; Deng, W.; Yao, S. One-Pot Preparation of Polymer−Enzyme−Metallic Nanoparticle Composite Films for High-Performance Biosensing of Glucose and Galactose. *Adv. Funct. Mater.* **2009**, 19, 1784−1791.

(19) Tan, Y. M.; Deng, W. F.; Li, Y. Y.; Huang, Z.; Meng, Y.; Xie, Q. J.; Ma, M.; Yao, S. Z. Polymeric Bionanocomposite Cast Thin Films with In Situ Laccase-Catalyzed Polymerization of Dopamine for Biosensing and Biofuel Cell Applications. *J. Phys. Chem. B* **2010**, 114, 5016−5024.

(20) Ball, V.; Del Frari, D.; Michel, M.; Buehler, M.; Toniazzo, V.; Singh, M.; Gracio, J.; Ruch, D. Deposition Mechanism and Properties of Thin Polydopamine Films for High Added Value Applications in Surface Science at the Nanoscale. *J. Bionanosci.* **2012**, 2, 16−34.

(21) Chen, C.; Fu, Y.; Xiang, C.; Xie, Q.; Zhang, Q.; Su, Y.; Wang, L.; Yao, S. Electropolymerization of Preoxidized Catecholamines on

Prussian Blue Matrix to Immobilize Glucose Oxidase for Sensitive Amperometric Biosensing. *Biosens. Bioelectron.* **2009**, 24, 2726−2729.

(22) Chen, C.; Wang, L.; Tan, Y.; Qin, C.; Xie, F.; Fu, Y.; Xie, Q.; Chen, J.; Yao, S. High-Performance Amperometric Biosensors and Biofuel Cell Based on Chitosan-Strengthened Cast Thin Films of Chemically Synthesized Catecholamine Polymers with Glucose Oxidase Effectively Entrapped. *Biosens. Bioelectron.* **2011**, 26, 2311−2316.

(23) Chen, S.-M.; Peng, K.-T. The Electrochemical Properties of Dopamine, Epinephrine, Norepinephrine, and their Electrocatalytic Reactions on Cobalt(II) Hexacyanoferrate Films. *J. Electroanal. Chem.* **2003**, 547, 179−189.

(24) Lynge, M. E.; van der Westen, R.; Postma, A.; Stadler, B. Polydopamine-a nature-inspired Polymer Coating for Biomedical Science. *Nanoscale* **2011**, 3, 4916−4928.

(25) Wang, Y.; Wang, S.; Niu, H.; Ma, Y.; Zeng, T.; Cai, Y.; Meng, Z. Preparation of Polydopamine Coated Fe_3O_4 Nanoparticles and their Application for Enrichment of Polycyclic Aromatic Hydrocarbons from Environmental Water Samples. *J. Chromatogr., A* **2013**, 1283, 20−26.

(26) Matsumoto, A.; Sato, N.; Kataoka, K.; Miyahara, Y. Noninvasive Sialic Acid Detection at Cell Membrane by Using Phenylboronic Acid Modified Self-Assembled Monolayer Gold Electrode. *J. Am. Chem. Soc.* **2009**, 131, 12022-+.

(27) Zayats, M.; Katz, E.; Willner, I. Electrical Contacting of Glucose Oxidase by Surface-Reconstitution of the Apo-Protein on a Relay-Boronic Acid-FAD Cofactor Monolayer. *J. Am. Chem. Soc.* **2002**, 124, 2120−2121.

(28) Huang, Y.; Qin, X.; Li, Z.; Fu, Y.; Qin, C.; Wu, F.; Su, Z.; Ma, M.; Xie, Q.; Yao, S.; Hu, J. Fabrication of a Chitosan/Glucose Oxidase-Poly(anilineboronic acid)-Aunano/Au-plated Au Electrode for Biosensor and Biofuel Cell. *Biosens. Bioelectron.* **2012**, 31, 357−362.

(29) Chen, C.; Xie, Q. J.; Yang, D. W.; Xiao, H. L.; Fu, Y. C.; Tan, Y. M.; Yao, S. Z. Recent Advances in Electrochemical Glucose Biosensors: A Review. *RSC Adv.* **2013**, 3, 4473−4491.

(30) Wang, J. Electrochemical Glucose Biosensors. *Chem. Rev.* **2007**, 108, 814−825.

(31) Fu, Y.; Chen, C.; Xie, Q.; Xu, X.; Zou, C.; Zhou, Q.; Tan, L.; Tang, H.; Zhang, Y.; Yao, S. Immobilization of Enzymes through One-Pot Chemical Preoxidation and Electropolymerization of Dithiols in Enzyme-Containing Aqueous Suspensions to Develop Biosensors with Improved Performance. *Anal. Chem.* **2008**, 80, 5829−5838.

(32) Fu, Y.; Li, P.; Bu, L.; Wang, T.; Xie, Q.; Chen, J.; Yao, S. Exploiting Metal-Organic Coordination Polymers as Highly Efficient Immobilization Matrixes of Enzymes for Sensitive Electrochemical Biosensing. *Anal. Chem.* **2011**, 83, 6511−6517.

(33) Fu, Y.; Zou, C.; Bu, L.; Xie, Q.; Yao, S. Novel Amperometric Aptasensor Based on Analyte-Induced Suppression of Enzyme Catalysis in Polymeric Bionanocomposites. *ACS Appl. Mater. Interfaces* **2013**, 5, 934−939.

(34) Lakshmi, D.; Bossi, A.; Whitcombe, M. J.; Chianella, I.; Fowler, S. A.; Subrahmanyam, S.; Piletska, E. V.; Piletsky, S. A. Electrochemical Sensor for Catechol and Dopamine Based on a Catalytic Molecularly Imprinted Polymer-Conducting Polymer Hybrid Recognition Element. *Anal. Chem.* **2009**, 81, 3576−3584.

(35) Fu, Y.; Li, P.; Bu, L.; Wang, T.; Xie, Q.; Xu, X.; Lei, L.; Zou, C.; Yao, S. Chemical/Biochemical Preparation of New Polymeric Bionanocomposites with Enzyme Labels Immobilized at High Load and Activity for High-Performance Electrochemical Immunoassay. *J. Phys. Chem. C* **2010**, 114, 1472−1480.

(36) Kohli, N.; Worden, R. M.; Lee, I. Direct Transfer of Preformed Patterned Bio-Nanocomposite Films on Polyelectrolyte Multilayer Templates. *Macromol. Biosci.* **2007**, 7, 789−797.

(37) Li, Y.; Qin, C.; Chen, C.; Fu, Y.; Ma, M.; Xie, Q. Highly Sensitive Phenolic Biosensor Based on Magnetic Polydopamine-Laccase-Fe_3O_4 Bionanocomposite. *Sens. Actuators, B* **2012**, 168, 46−53.

(38) Li, Y.; Tan, Y.; Deng, W.; Xie, Q.; Zhang, Y.; Chen, J.; Yao, S. Electropolymerization of Catecholamines after Laccase-Catalyzed

Preoxidation to Efficiently Immobilize Glucose Oxidase for Sensitive Amperometric Biosensing. *Sens. Actuators., B* **2010**, *151*, 30−38.

(39) Tan, Y.; Deng, W.; Ge, B.; Xie, Q.; Huang, J.; Yao, S. Biofuel Cell and Phenolic Biosensor Based on Acid-Resistant Laccase-Glutaraldehyde Functionalized Chitosan-Multiwalled Carbon Nanotubes Nanocomposite Film. *Biosens. Bioelectron.* **2009**, *24*, 2225−2231.

(40) Tan, Y.; Xie, Q.; Huang, J.; Duan, W.; Ma, M.; Yao, S. Study on Glucose Biofuel Cells Using an Electrochemical Noise Device. *Electroanalysis* **2008**, *20*, 1599−1606.

(41) Zhang, J.; Song, S.; Wang, L.; Pan, D.; Fan, C. A Gold Nanoparticle-Based Chronocoulometric DNA Sensor for Amplified Detection of DNA. *Nat. Protoc.* **2007**, *2*, 2888−2895.

(42) Xiao, Y.; Lai, R. Y.; Plaxco, K. W. Preparation of Electrode-Immobilized, Redox-Modified Oligonucleotides for Electrochemical DNA and Aptamer-Based Sensing. *Nat. Protoc.* **2007**, *2*, 2875−2880.

(43) Xie, Q.; Xiang, C.; Yuan, Y.; Zhang, Y.; Nie, L.; Yao, S. A Novel Dual-Impedance-Analysis EQCM System–Investigation of Bovine Serum Albumin Adsorption on Gold and Platinum Electrode Surfaces. *J. Colloid Interface Sci.* **2003**, *262*, 107−115.

(44) Su, Y.; Xie, Q.; Chen, C.; Zhang, Q.; Ma, M.; Yao, S. Electrochemical Quartz Crystal Microbalance Studies on Enzymatic Specific Activity and Direct Electrochemistry of Immobilized Glucose Oxidase in the Presence of Sodium Dodecyl Benzene Sulfonate and Multiwalled Carbon Nanotubes. *Biotechnol. Prog.* **2008**, *24*, 262−272.

(45) Yang, Z.; Zhang, C.; Zhang, J.; Bai, W. Potentiometric Glucose Biosensor Based on Core-Hell Fe_3O_4-Enzyme-Polypyrrole Nanoparticles. *Biosens. Bioelectron.* **2014**, *51*, 268−273.

(46) Dey, R. S.; Raj, C. R. Redox-Functionalized Graphene Oxide Architecture for the Development of Amperometric Biosensing Platform. *ACS Appl. Mater. Interfaces* **2013**, *5*, 4791−4798.

(47) Levis, J. T.; Ford, J. B.; Kuo, A. M. Intracranial Hemorrhage after Prehospital Administration of Intramuscular Epinephrine. *J. Emerg. Med.* **2011**, *40*, e107−e110.

(48) Thibault, S.; Aubriet, H.; Arnoult, C.; Ruch, D. Gold Nanoparticles and a Glucose Oxidase Based Biosensor: An Attempt to Follow-Up Aging by XPS. *Microchim. Acta* **2008**, *163*, 211−217.

(49) Zhang, S.; Wang, N.; Yu, H.; Niu, Y.; Sun, C. Covalent Attachment of Glucose Oxidase to an Au Electrode Modified with Gold Nanoparticles for Use as Glucose Biosensor. *Bioelectrochemistry* **2005**, *67*, 15−22.

(50) Luo, X.-L.; Xu, J.-J.; Du, Y.; Chen, H.-Y. A Glucose Biosensor Based on Chitosan-Glucose Oxidase-Gold Nanoparticles Biocomposite Formed by One-Step Electrodeposition. *Anal. Biochem.* **2004**, *334*, 284−289.

(51) Shan, C.; Yang, H.; Han, D.; Zhang, Q.; Ivaska, A.; Niu, L. Graphene/AuNPs/Chitosan Nanocomposites Film for Glucose Biosensing. *Biosens. Bioelectron.* **2010**, *25*, 1070−1074.

(52) Palanisamy, S.; Karuppiah, C.; Chen, S.-M. Direct Electrochemistry and Electrocatalysis of Glucose Oxidase Immobilized on Reduced Graphene Oxide and Silver Nanoparticles Nanocomposite Modified Electrode. *Colloids Surf., B* **2014**, *114*, 164−169.

(53) Rakhi, R. B.; Sethupathi, K.; Ramaprabhu, S. A Glucose Biosensor Based on Deposition of Glucose Oxidase onto Crystalline Gold Nanoparticle Modified Carbon Nanotube Electrode. *J. Phys. Chem. B* **2009**, *113*, 3190−3194.

(54) Zhang, Z. J.; Xie, Y. B.; Liu, Z.; Rong, F.; Wang, Y.; Fu, D. G. Covalently Immobilized Biosensor Based on Gold Nanoparticles Modified TiO_2 Nanotube Arrays. *J. Electroanal. Chem.* **2011**, *650*, 241−247.

(55) Lang, Q.; Yin, L.; Shi, J.; Li, L.; Xia, L.; Liu, A. Co-Immobilization of Glucoamylase and Glucose Oxidase for Electrochemical Sequential Enzyme Electrode for Starch Biosensor and Biofuel Cell. *Biosens. Bioelectron.* **2014**, *51*, 158−163.

(56) Korani, A.; Salimi, A. Fabrication of High Performance Bioanode Based on Fruitful Association of Dendrimer and Carbon Nanotube Used for Design O_2/Glucose Membrane-Less Biofuel Cell with Improved Bilirubine Oxidase Biocathode. *Biosens. Bioelectron.* **2013**, *50*, 186−193.

(57) Yehezkeli, O.; Tel-Vered, R.; Raichlin, S.; Willner, I. Nano-engineered Flavin-Dependent Glucose Dehydrogenase/Gold Nanoparticle-Modified Electrodes for Glucose Sensing and Biofuel Cell Applications. *ACS Nano* **2011**, *5*, 2385−2391.

(58) Scherbahn, V.; Putze, M. T.; Dietzel, B.; Heinlein, T.; Schneider, J. J.; Lisdat, F. Biofuel Cells Based on Direct Enzyme−Electrode Contacts Using PQQ-Dependent Glucose Dehydrogenase/Bilirubin Oxidase and Modified Carbon Nanotube Materials. *Biosens. Bioelectron.* **2014**, *61*, 631−638.